

# Transport limitations on development times of LIGA PMMA resists

S. K. Griffiths, R. H. Nilson

335

**Abstract** Analytical and numerical methods are employed to investigate the role of PMMA fragment transport in resist development for the LIGA process. We demonstrate that the overall development time can be expressed as the sum of the kinetic-limited development time and a time for fragment transport. The kinetic-limited time depends only on the resist thickness, dose profile and development temperature and is independent of feature size. The transport time grows as the square of the resist thickness and falls inversely with the Sherwood number. A new analytical model describing the Sherwood number for forced convective transport in deep cavities is also developed. This model, applicable to both resist development and electroforming, is compared with numerical simulations and with data previously reported. Based on this model, we find that forced convective transport can significantly reduce development times only for features having an aspect ratio less than about five. Acoustic agitation is also discussed, and sample calculations of the development time are presented for both forced convective transport and acoustic agitation over a wide range of feature sizes.

## 1 Introduction

The LIGA process [1, 2] employs synchrotron X-ray lithography to expose a thick PMMA resist through a patterned absorber mask. Such exposure reduces the resist molecular weight by main-chain scission of the PMMA below open portions of the absorber [3]. The resulting fragments of PMMA are dissolved during subsequent development to produce a (usually) two-dimensional

structure of fixed thickness. This may be used as a finished plastic part, or may serve as a mold for fabricating an inverse metal structure via electrodeposition.

This process is capable of producing structures having feature heights up to several millimeters and feature aspect ratios of 50 or more. While such structures are possible, the successful development of exposed resists becomes difficult and time consuming as both the resist thickness and feature aspect ratio increase. Development times for a 200  $\mu\text{m}$  resist thickness are typically less than 2 h for all aspect ratios, but increase to nearly 20 h for high aspect ratios at a resist thickness of 1 mm. The development of thick resists is particularly problematic for resists patterned with both large and small features since features of widely varying size generally develop at widely disparate rates. The resulting disparities in development times may lead to a loss of structure accuracy or, in the worst of cases, to the detachment of small posts or webs due to lateral dissolution near the PMMA substrate [4].

These development problems arise from limitations on the development rate imposed by transport processes [5–7]. Development of exposed PMMA requires the release of PMMA fragments at the dissolution interface as well as the transport of these fragments out of each feature and away from the resist. Either the dissolution kinetics or the transport rate may thus determine the local development rate and overall development times.

The transport of fragments along a feature may occur both by diffusion and by convective motion. Diffusive transport rates are relatively low due to the high molecular weights typical of PMMA fragments. Convective transport rates are usually much larger, even for fluid (developer) speeds as low as 1  $\mu\text{m/s}$ , but convective motion is difficult to produce deep in features of high aspect ratio [8]. As a result, small features of high aspect ratio tend to develop slowly at a diffusion-limited rate, while larger features, having low aspect ratios, tend to develop more quickly at the kinetic-limited rate of PMMA dissolution.

Here we analyze diffusive and convective transport of PMMA fragments and examine the effect of such transport on resist development times. Both forced convection and acoustic agitation are considered. As part of this study, we develop a new model describing forced convective transport in deep features. This model is applicable to both circular and rectangular features and is suitable for use at all aspect ratios. The results of the model are presented first in the form of the local Sherwood number based on the instantaneous feature depth. The local Sherwood number is then integrated over the completed feature

Received: 10 August 2001/Accepted: 24 September 2001

S. K. Griffiths (✉), R. H. Nilson  
Chemical and Materials Process Modeling Department,  
Sandia National Laboratories,  
Livermore, California 94551-0969, USA  
E-mail: skgriff@sandia.gov

This work was funded in part by the NNSA Advanced Development and Production Technology (ADAPT) program and in part by the DOE Accelerated Strategic Computing Initiative (ASCI) applications program. Sandia National Laboratories is operated by Sandia Corporation for the United States Department of Energy under contract DE-AC04-94AL85000.

This paper was presented at the Fourth International Workshop on High Aspect Ratio Microstructure Technology HARMST 2001 in June 2001.

depth to yield the mean Sherwood number as a function of the final aspect ratio. Although the focus of this work is resist development, the transport model and resulting Sherwood numbers are also applicable to electrodeposition. Sample calculations of development times for both forced convection and acoustic agitation are also presented and discussed.

## 2 Development times

Consider the development of a single isolated feature where the dissolution front is advancing into the PMMA. PMMA fragments are released at the dissolution surface at a rate that is proportional to the product of the front speed,  $U$ , and the solid density of PMMA,  $\rho_s = 1.2 \text{ g/cm}^3$ . In quasi-steady state, species conservation then requires that the mass flux of PMMA fragments away from the dissolution surface just equals the fragment transport rate between the dissolution front and the open top of the feature. If we now assume that the kinetic-limited dissolution rate,  $R$ , is reversible and that this reversible reaction is first-order in the fragment mass density,  $c$ , in the developer adjacent to the dissolution front, then this equilibrium between the kinetic dissolution rate and the fragment transport rate can be expressed as

$$\rho_s U = R(\rho_s - c) = \frac{cShD}{y} \quad (1)$$

where  $D$  is the fragment diffusivity in the developer,  $y$  is the instantaneous feature depth and  $Sh$  is the Sherwood number also based on the instantaneous feature depth. The Sherwood number indicates the magnitude of the PMMA fragment transport rate relative to that by diffusion alone. Its value is  $Sh = 1$  for diffusive transport. More generally, Sherwood numbers for convective transport must be computed from the multi-dimensional flow field within the feature.

Eliminating the fragment density,  $c$ , between the two right-hand expressions of Eq. (1), we find that the overall development rate can be expressed as

$$U = R(1 - c^*), \quad c^* = \frac{yR}{yR + ShD} \quad (2)$$

such that the development rate  $U$  is limited by both dissolution kinetics and fragment transport. The total development time,  $t$ , can now be written in terms of the local development rate

$$t = \int_0^h \frac{dy}{U} \quad (3)$$

where  $h$  is the final feature depth or, equivalently, the resist thickness.

From the form of Eq. (2), we see that the integral above can be split into two contributions. The first contribution is that due to the kinetic-limited development rate; the second is due to the finite rate of fragment transport. As a result, the total development time can be expressed as the

simple sum of the kinetic-limited development time,  $t_0$ , and the characteristic time for transport,  $\delta t$ . That is,

$$t = t_0 + \delta t, \quad t_0 = \int_0^h \frac{dy}{R} \quad \text{and} \quad \delta t = \int_0^h \frac{y dy}{DSh} \quad (4)$$

The last of these expressions can also be written in terms of an average Sherwood number,  $\overline{Sh}$ .

$$\delta t = \frac{h^2}{2D\overline{Sh}}, \quad \frac{1}{\overline{Sh}} = \frac{2}{h^2} \int_0^h \frac{y dy}{Sh} = \frac{2}{A_f^2} \int_0^{A_f} \frac{A dA}{Sh} \quad (5)$$

Again,  $Sh$  is the instantaneous Sherwood number. Its value thus depends on the instantaneous depth,  $y$ , through its dependence on the aspect ratio, which increases continuously through the course of development. To compute the integral yielding  $\delta t$  or  $\overline{Sh}$ , it is therefore useful to make the substitution  $y = hA/A_f$  where  $A$  is the instantaneous aspect ratio and  $A_f$  is the aspect ratio upon complete development of the feature. This substitution yields the second form of the integral. Note that  $\overline{Sh} = Sh$  if the value of the Sherwood number is independent of the aspect ratio. This occurs in the important special case of  $Sh = 1$ , corresponding to diffusion-limited transport.

The kinetic-limited development rate depends only on the dose and development temperature, so  $t_0$  in Eq. (4) is independent of both the feature size and aspect ratio provided that secondary radiation is negligible. As such, the difference in development times for two features of differing size on the same resist is given by

$$\Delta t_{1,2} = t_1 - t_2 = \delta t_1 - \delta t_2 = \frac{h^2}{2D} \left( \frac{1}{\overline{Sh}_1} - \frac{1}{\overline{Sh}_2} \right) \quad (6)$$

Note that this result is (nearly) independent of the absorbed dose and depends only weakly on the developer temperature through the fragment diffusivity. It does, however, depend strongly on any developer motion within the feature through the two Sherwood numbers. Also note that the maximum possible differential in development times is  $\Delta t_{1,2} = h^2/2D$  based on the disparity between the extremes of diffusion-limited development ( $\overline{Sh}_1 = 1$ ) and kinetic-limited development ( $\overline{Sh}_2 \rightarrow \infty$ ).

## 3 Forced convective transport

Sherwood numbers are determined by analyzing the spatial distribution of PMMA fragments resulting from the flow field inside and outside the feature. Here we examine the case of forced convective transport. Such transport arises when the developer outside a feature is driven by stirring or by moving the resist in a quiescent bath. It also arises in some schemes intended to reduce development (or plating) times by increasing the Sherwood number. These include paddle cells, flow-through cells and schemes based on the flow induced by a rotating disk.

Forced convection over the top of a feature produces a series of counter-rotating cells along the feature height. Each cell occupies the full feature width, but only a fraction of the feature height. The number of cells formed depends on the feature aspect ratio and a limiting aspect ratio for

each cell. Several previous studies have demonstrated that the cell aspect ratio generally does not exceed about 1.4 [8–10]. Thus features having aspect ratios below about 1.4 will contain a single cell. Features having aspect ratios between about 1.4 and about 2.8 will exhibit two cells, and so on.

Near the top and bottom of each of these cells, there exists a roughly horizontal line along which the vertical component of the fluid velocity vanishes. This is the streamline dividing adjacent cells. All species transport across this line must occur by diffusion alone, giving rise to boundary layers in the spatial distribution of the fragment concentration. Such boundary layers are located between each pair of adjacent cells and at the top and bottom of a feature. The number of cells,  $N_c$ , and number of boundary layers,  $N_b$ , can thus be expressed as

$$N_c = \left\lceil \frac{A}{1.4} \right\rceil \quad \text{and} \quad N_b = N_c + 1 \quad (7)$$

where again  $A$  is the instantaneous feature aspect ratio. The number of cells is obtained by rounding the ratio  $A/1.4$  upward to the nearest integer, as indicated by the floor brackets.

Each of these boundary layers represents a resistance to fragment transport upward along the feature, and the magnitude of the resistance is the inverse of the Sherwood number. As these resistances appear in series, the overall resistance is obtained by a simple sum analogous to that of electrical resistors. For transport, this overall resistance can be expressed in terms of the overall Sherwood number,  $Sh$ , based on the feature depth.

$$\frac{1}{Sh} = \frac{1}{N_b} \sum_{i=1}^{N_b} \frac{1}{Sh_i} \quad (8)$$

where  $Sh_i$  is the local Sherwood number associated with each boundary layer. The convective portion of the local Sherwood number,  $Sh_i - 1$ , can be expressed in a similar manner as an overall resistance due to the series resistances in the low and high Peclet number limits. That is,

$$\frac{1}{Sh_i - 1} = \frac{1}{Sh_{i,0} - 1} + \frac{1}{Sh_{i,\infty} - 1} \quad (9)$$

where  $Sh_{i,0}$  is the Sherwood number in the low Peclet number regime, and  $Sh_{i,\infty}$  is that in the high Peclet number limit. Note that the form of Eqs. (8) and (9) takes into account that a boundary layer thickness cannot exceed the adjacent cell height, ensuring a minimum possible Sherwood number of unity for each cell and for the feature.

The Peclet number,  $Pe$ , is the product of the Reynolds and Schmidt numbers. Schmidt numbers for ions in an aqueous solution are usually on the order of  $10^3$ , while those for fragments in developer are order  $10^5$ . Thus the Reynolds number must always be small at low Peclet numbers for the problems of interest here. In this case, the Sherwood number for most geometries grows in proportion to the square of the Peclet number [11]. At high Peclet numbers, things are bit more complicated. If the Reynolds number is small, the Sherwood number again grows in proportion to some power of the Peclet number, and this

power depends mostly on the nature of the boundary layer. Fluid–solid boundary layers tend to exhibit a one-third power; fluid–fluid layers usually exhibit a one-half power [11, 12]. At higher Reynolds numbers, the Sherwood number no longer depends strictly on the Peclet number, but instead grows in proportion to some power of the Reynolds number and in proportion to the third-root of the Schmidt number [11, 12]. Here we assume, for the sake of simplicity, that all high Peclet number transport occurs at low Reynolds numbers and that fluid–fluid boundaries are predominant. Under these conditions, the local Sherwood numbers at low and high Peclet numbers can be written as

$$Sh_{i,0} - 1 = aPe_i^2 \quad \text{and} \quad Sh_{i,\infty} - 1 = bPe_i^{1/2} \quad (10)$$

where  $Pe_i$  is the local Peclet number associated with the  $i$ th boundary layer. This Peclet number is based on the local characteristic fluid speed and the hydraulic diameter of the feature where the hydraulic diameter is four times the cross-section area divided by the wetted perimeter. The hydraulic diameter of a circular feature is thus the feature diameter,  $d_H = d$ ; that of a wide channel is twice the channel width,  $d_H = 2w$ . Based on these definitions, the local Peclet number is given by

$$Pe_i = \frac{u_i d_H}{D} = \frac{u_i d}{D} = \frac{2u_i w}{D} \quad (11)$$

The overall characteristic fluid speed for flow across a feature is the product of the feature width,  $w$  or  $d$ , and the shear rate,  $\gamma$ , at the top surface just upstream of the feature. That is,

$$u_{\text{ref}} = \gamma d = \gamma w, \quad \gamma = \frac{\partial u}{\partial y} \quad \text{at} \quad y = 0 \quad (12)$$

Based on previous finite-difference numerical results [9, 10], the characteristic speed at the top boundary layer ( $i = 1$ ) is about 10% of the reference speed,  $u_{\text{ref}}$ . For each subsequent boundary layer ( $i > 1$ ), the characteristic speed drops by very nearly two orders-of-magnitude. Thus, the local Peclet number at the  $i$ th boundary layer can be expressed as

$$Pe_i = Pe_\gamma e^{-2.3(2i-1)}, \quad Pe_\gamma = \frac{\gamma d^2}{D} = \frac{2\gamma w^2}{D} \quad (13)$$

These two definitions of the Peclet number apply to circular and rectangular features, respectively.

The shear rate  $\gamma$  appearing in the Peclet number above is readily calculated for a variety of conditions. For streaming flow across a flat plate, the well-known result is [12]

$$\gamma = 0.33 \sqrt{\frac{u^3}{\nu L}} \quad (14)$$

where  $u$  is the free-stream fluid speed,  $\nu$  is the fluid viscosity and  $L$  is the position downstream of the leading edge. For low Reynolds number, fully-developed flow between parallel plates, the shear rate along either plate is given by

$$\gamma = \frac{8u}{W} \quad (15)$$

where  $u$  is the mean fluid speed, and  $W$  is the distance between the two plates. Lastly, the shear rate on a rotating disk is given by [12]

$$\gamma = 0.80 \sqrt{\frac{r^2 \omega^3}{\nu}} \quad (16)$$

where  $r$  is the radial position, and  $\omega$  is the angular speed of rotation.

This analytical model describing the Sherwood number contains just two unknown parameters,  $a$  and  $b$  appearing Eq. (10). To obtain values for these, we have fit the model to the results of numerical simulations of forced convective transport in which the shear rate is specified at the top surface upstream of a rectangular feature [10]. The flow is directed across the narrow dimension such that the problem is two-dimensional. The best-fit values obtained for aspect ratios of one and two are  $a = 0.03$  and  $b = 0.25$ .

A comparison between the Sherwood numbers computed numerically and those given by the analytical model is shown in Fig. 1. Here we see that this simple analytical model closely reproduces a complex dependence of the Sherwood number on the Peclet number and aspect ratio. For an aspect ratio of  $A = 1$ , the Sherwood number rises smoothly from  $Sh = 1$  and eventually grows as the square-root of the Peclet number as the Peclet number becomes large. We see a very different, wavy behavior at an aspect ratio of  $A = 2$ . In this case, the Sherwood number rises somewhat abruptly from about 1.3 to about 2 between  $Pe_\gamma = 10^3$  and  $10^4$ . Then, between  $Pe_\gamma = 10^4$  and  $10^5$ , it remains relatively constant on an inclined plateau. Finally, the Sherwood number again increases as the Peclet number exceeds  $10^5$ . Similar behavior also occurs at higher aspect ratios, with the number of plateaus growing in proportion to the number of cells.

To benchmark this model, we have also compared its results with Sherwood numbers previously measured in the context of the electrodeposition [13]. These experiments were performed using circular features located at a fixed radial position of  $r = 3$  mm on a rotating disk. The

rotational speed was varied up to 1000 rpm. Feature diameters varied from 10 to 200  $\mu\text{m}$ ; depths ranged for 100–350  $\mu\text{m}$ , yielding aspect ratios between 0.5 and 20. The Sherwood numbers measured in this study were reported as a function of a Reynolds number,  $Re_\omega$ , based on the angular speed, radial position on the disk and the feature size. This Reynolds number can be converted to the Peclet number used here via Eq. (16). The result is

$$Pe_\gamma = \frac{\gamma d^2}{D} = 0.80 \sqrt{\frac{d}{r}} Re_\omega^{3/2} Sc, \quad Re_\omega = \frac{r\omega d}{\nu} \quad (17)$$

The Schmidt number used in the conversion is  $Sc = \nu/D = 1400$  based on  $\nu = 1.1 \times 10^{-6} \text{ m}^2/\text{s}$  and  $D = 0.8 \times 10^{-9} \text{ m}^2/\text{s}$ .

The results of this comparison are shown in Fig. 2. Symbols represent the data; the curves represent results of the analytical model. The solid symbols are for aspect ratios of  $A = 1, 2, 4, 7$  and 20, corresponding to the five-labeled curves. All data for  $A = 20$  lie below  $Pe_\gamma = 10^3$ . The open symbols are for aspect ratios of 0.5 and 1.7. Note that the analytical results in Figs. 1 and 2 are identical; that is, the two parameters  $a = 0.03$  and  $b = 0.25$  are the same in each case. The agreement between the model and data is exceptionally good considering that the model was not fit to this data in any way. The largest relative error between the measured and calculated Sherwood numbers is less than 20% for the aspect ratios of 1, 2, 4, 7 and 20.

The data in Fig. 2 also seem to confirm several assumptions implicit in the model. First, there appears to be little difference between the Sherwood numbers at aspect ratios of 0.5 and 1 (both  $N_c = 1$ ). Similarly, the measured values for  $A = 1.7$  are close to those for  $A = 2$  (both  $N_c = 2$ ), at least up to Peclet numbers of about  $10^5$ . These two observations tend to support the notion that the number of cells and boundary layers is more important than the aspect ratio in determining the Sherwood number. Second, the Sherwood numbers measured at  $A = 1$  employed feature diameters of both 100 and 200  $\mu\text{m}$ ; those for  $A = 2$  used features of both 50 and

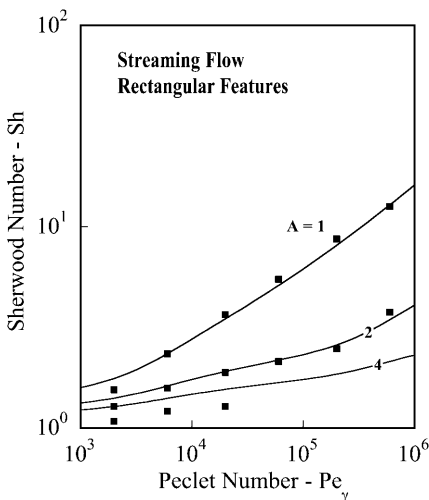


Fig. 1. Analytical model of Sherwood number as a function of the Peclet number and aspect ratio. Symbols represent Sherwood numbers computed numerically

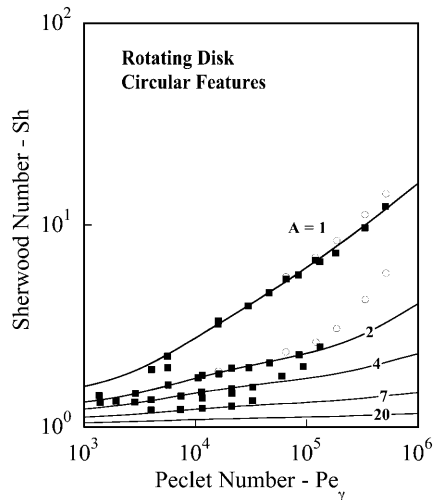


Fig. 2. Comparison of analytical model with measured values of the Sherwood number for circular features on a rotating disk. Open symbols represent  $A = 0.5$  and 1.7

100  $\mu\text{m}$ . In the original paper, the Sherwood number was plotted relative to the Reynolds Number,  $Re_\omega$ , and the effect of the feature size was clearly evident. In Fig. 2, however, no such effect is seen. This supports the notion that the Peclet number,  $Pe_\gamma$ , which varies as the square of the feature size, is indeed the appropriate parameter governing the Sherwood number. Finally, we see in Fig. 2 a tendency for the model to under-predict the measured Sherwood numbers when the Peclet number is very large. Recall that the high Peclet number correlation used in Eq. (10) applies to high Peclet numbers only when the Reynolds number is small. Thus the assumption of a small Reynolds number seems appropriate for most conditions of practical interest. This assumption will break down, however, for Reynolds numbers much above one. The corresponding Peclet number is about  $10^3$  for electrodeposition ( $Sc \sim 10^3$ ) and about  $10^5$  for development ( $Sc \sim 10^5$ ).

We note that the Sherwood number for forced convection is strongly dependent on the number of cells, so the aspect ratio and Peclet number may not uniquely determine its value. There is always some uncertainty in the number of cells that will result for a given aspect ratio, and this uncertainty grows for aspect ratios near multiples of 1.4. Near these values, the flow field may not even be unique. In addition, weak secondary influences such as buoyancy may alter the cell structure to give more or fewer cells for a given feature geometry [10]. The number of cells may also be influenced by initial conditions or by the geometry surrounding a feature. This uncertainty in the number of cells gives rise to uncertainty in the Sherwood number. Sherwood numbers may thus change abruptly with small changes in the aspect ratio or may even have multiple values for a single geometry. Such unpredictable behavior should be most apparent at aspect ratios below about five since an increase or decrease of one cell represents a larger relative uncertainty in the cell count when the number of cells is small.

Finally, we note that the correlation above should apply to both circular and rectangular features (holes and trenches) if the Peclet number is based on the hydraulic diameter. For rectangular features, however, these results apply only to cases in which the external flow directly crosses the smaller dimension. This analysis is simply not applicable to wide rectangular features for cases in which there is significant external flow parallel to the longer dimension.

#### 4 Sonic agitation

Unlike forced convective transport, acoustic agitation produces a pair of counter-rotating cells that each occupies half of the feature width but span the full feature height. Boundary layers thus arise only at the top and bottom of the feature. Further, the characteristic fluid speeds at the top and bottom boundary layers are the same, so each boundary layer offers substantially the same resistance to species transport. Because of this, the overall Sherwood number can be expressed in terms of just the high and low Peclet number behaviors. That is,

$$\frac{1}{Sh - 1} = \frac{1}{Sh_0 - 1} + \frac{1}{Sh_\infty - 1} \quad (18)$$

$$Sh_0 - 1 = 0.022Pe_a^2 \quad \text{and} \quad Sh_\infty - 1 = 2.4APe_a^{1/3} \quad (19)$$

The Peclet number for sonic agitation is based on the characteristic acoustic velocity and the feature width. This can be written as

$$Pe_a = \frac{Iw}{10\rho c^2 D} \quad (20)$$

where  $I$  is the acoustic intensity,  $\rho \sim 10^3 \text{ kg/m}^3$  is the fluid density and  $c \sim 1500 \text{ m/s}$  is the speed of sound in the fluid. This model for acoustic agitation was reported and compared with experimental results in a previous study [14].

#### 5 Mean Sherwood numbers

Here we are interested in the mean Sherwood number and how its value affects development times for features of various size, but all located on a single substrate. The resist thickness is fixed in the LIGA process, so variations in final aspect ratio are equivalent to variations in feature size. Since the Sherwood number depends on the feature size through the Peclet number, a variation in feature size requires a change in either the shear rate,  $\gamma$ , or the acoustic intensity,  $I$ , to maintain a fixed Peclet number. This is in conflict, however, with the notion of a single substrate because the shear rate or acoustic intensity is uniform over all features, at least for features located near one another. As a result, a fixed Peclet number does not correctly represent the case in which features of various aspect ratio reside on a single substrate.

To address this properly, we need to consider that the Peclet number is proportional to the square of the feature size for forced convection and varies linearly with feature size for acoustic agitation. As a result, the product of the aspect ratio and the Peclet number  $A_f^2 Pe_\gamma$  is fixed for forced convection when both the shear rate and resist thickness are constant. The term  $A_f Pe_a$  plays a similar role for acoustic agitation; a fixed value of this product corresponds to a fixed intensity and fixed resist thickness. Thus by specifying both the aspect ratio and either  $A_f^2 Pe_\gamma$  or  $A_f Pe_a$ , the Peclet number appropriate for features on a common substrate is also determined. For each aspect ratio, this Peclet number can then be used to compute the mean Sherwood number via Eq. (5). Here, the required integral is evaluated using a numerical quadrature routine. This numerical approach is needed for the equations governing forced convection, though the integral can also be obtained analytically for the simpler equations governing acoustic agitation.

Figure 3 shows mean Sherwood numbers for forced convection as a function of the feature aspect ratio for several values of  $A_f^2 Pe_\gamma$ . The values shown were selected to span the range of conditions of interest for LIGA development. For example,  $A_f^2 Pe_\gamma = 10^8$  corresponds to  $\gamma = 1000$  for a diffusivity of  $D = 10^{-11} \text{ m}^2/\text{s}$  and resist thickness of  $h = 1 \text{ mm}$ . By Eq. (14), this shear rate at a

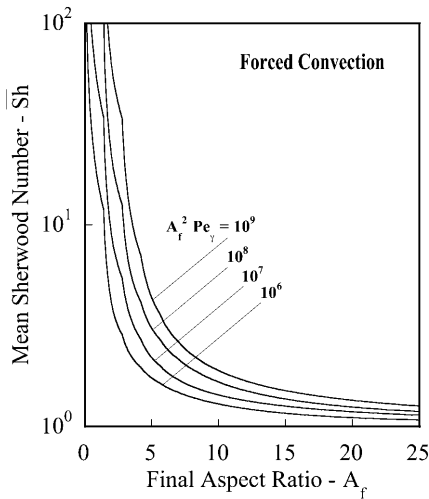


Fig. 3. Mean Sherwood numbers fall rapidly with increasing aspect ratio even when Peclet numbers are very large. The product  $A_f^2 Pe_\gamma$  depends on the resist thickness, but is independent of feature size

distance  $L = 50$  mm from the leading edge of the substrate requires a free-stream developer speed of about  $u = 0.8$  m/s based on a viscosity of  $\nu = 10^{-6}$  m<sup>2</sup>/s. This is quite high, though not unrealistic. For flow between two plates spaced at  $W = 10$  mm and the same properties and resist thickness, the required mean fluid speed is  $u = 1.2$  m/s. Similarly, for features located on a rotating disk at  $r = 50$  mm, the required speed of rotation to obtain  $\gamma = 1000$  is about 80 rpm. Again, this is fairly high, though not unreasonable. Thus the value  $A_f^2 Pe_\gamma = 10^9$  shown in Fig. 4 will be difficult to obtain, and the high speeds required are likely to damage free-standing features near the end of the development period. Note that the wavy character of these curves represents the same waviness seen early in Figs. 1 and 2. The kinks arise at aspect ratios that are integer multiples of 1.4, the presumed maximum aspect ratio of fluid cells within a feature.

We see in Fig. 3 that the mean Sherwood number falls very rapidly with increasing aspect ratio. Even for  $A_f^2 Pe_\gamma = 10^9$ , the Sherwood number exceeds 10 only for aspect ratios up to about three. It falls to  $\bar{Sh} \approx 4$  at an aspect ratio of five and is less than two for aspect ratios greater than 10.

Figure 4 shows computed mean Sherwood numbers for acoustic agitation as a function of the aspect ratio. Here the value of  $A_f Pe_a$  is fixed, and again the values shown were selected to span the parameter range of interest. Based on a resist thickness of  $h = 1$  mm and a diffusivity of  $D = 10^{-11}$  m<sup>2</sup>/s, these values correspond to acoustic intensities of  $I = 2.2, 4.5, 9$  and  $18$  W/cm<sup>2</sup>. Here we see that mean Sherwood numbers for acoustic agitation exhibit a maximum at some finite aspect ratio and that the aspect ratio yielding the maximum increases about linearly with increasing  $A_f Pe_a$ . We also see that the Sherwood numbers are very sensitive to  $A_f Pe_a$  over the full range of aspect ratios. This is in contrast to the results for forced convection. Finally, we see that the mean Sherwood numbers can be very large even at large aspect

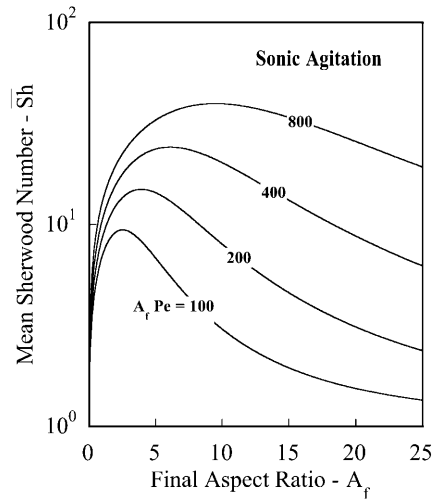


Fig. 4. Mean Sherwood numbers for acoustic agitation may remain large even for aspect ratios of 25 at sufficient acoustic intensities. The product  $A_f Pe$  is independent of feature size

ratios, provided that the acoustic intensity is sufficiently high.

## 6 Sample calculations

To illustrate the impact of transport on the development process, we have made some sample calculations of overall development times under conditions of both forced convection and acoustic agitation. These simulations are based on exposures performed at SSRL ( $\lambda_c = 2.66$  Å) using a 100 μm silicon mask membrane, a fixed bottom-surface dose of 5.2 kJ/cm<sup>3</sup>, GG developer, a development temperature of 25 °C, and a fixed fragment diffusivity of  $10^{-11}$  m<sup>2</sup>/s. The kinetic-limited development rate is taken as

$$R = G \frac{(Q/B)^C}{1 + (Q/B)^C} e^{-\frac{E_a}{R}(\frac{1}{T} - \frac{1}{T_r})}, \quad E_a = \frac{\alpha}{1 + (Q/\beta)^\kappa} \quad (21)$$

and  $Q$  is the local absorbed dose;  $T_r = 308$  K (35 °C) is a reference temperature, and  $R = 8.314$  J/mol is the ideal gas constant. Parameters for the development rate are  $G = 14$  μm/min,  $B = 4.7$  kJ/cm<sup>3</sup>, and  $C = 3.8$ ; those for the activation energy are  $\alpha = 140$  kJ/mol,  $\beta = 8.3$  kJ/cm<sup>3</sup>, and  $\kappa = 2.4$  [15]. This expression yields kinetic-limited development rates that are just slightly below measured rates previously reported [16].

Results for forced convection are shown in Fig. 5 as a function of the PMMA thickness for various feature sizes. The results are obtained by integrating the development front location forward in time, using the local absorbed dose and local Sherwood number to compute the instantaneous development speed. The integration is continued until the dissolution front reaches the substrate, yielding the total development time. In all cases, transport within the features is driven by a streaming flow over the resist. The speed is taken as  $u = 1$  m/s, and the features are assumed to be located at  $L = 50$  mm from the leading edge. By Eq. (14), these yield  $\gamma = 1480$  s<sup>-1</sup> for a viscosity of  $10^{-6}$  m<sup>2</sup>/s.

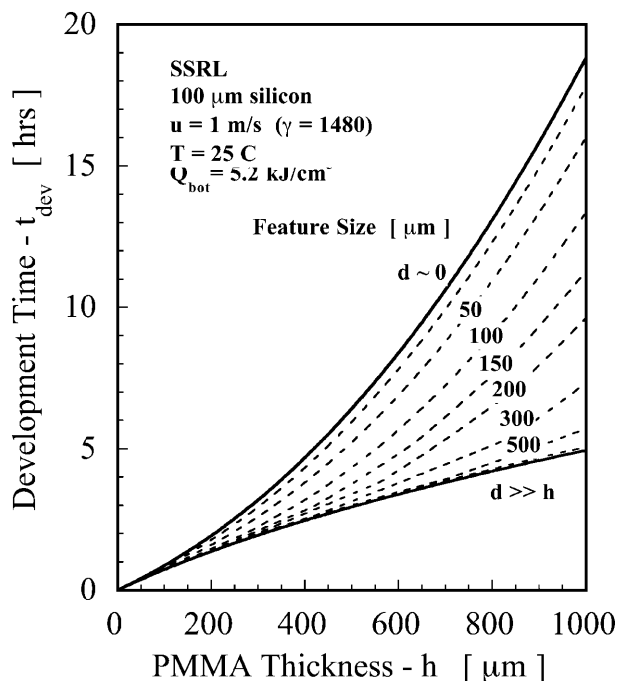


Fig. 5. Development times for forced convection over PMMA surface. Time differential between small and large features grows large when the resist thickness is large and aspect ratios exceed about four

Here we see that the development time for very small features ( $d \sim 0$ ) is controlled by diffusion, while those for very large features ( $d \gg h$ ) are controlled by the kinetics of dissolution. These diffusion-limited and kinetic-limited values are shown by the two solid curves. Note that the kinetic-limited development times do not increase linearly with the resist thickness because the bottom dose is fixed and the top dose thus increases with increasing thickness. As expected, the disparity in development times between these two limits grows precisely in proportion to the square of the PMMA thickness. Development times are thus similar for all aspect ratios when the resist thickness is small, less than about 200  $\mu\text{m}$ . As the thickness increases, however, the diffusion-limited and kinetic-limited development times rapidly diverge. Forced convection reduces development times to roughly the kinetic-limited values only for aspect ratios up to about one, and significant reductions in the development time are obtained only for aspect ratios less than three or four. For aspect ratios above 10, forced convection provides little benefit in reducing development times. Note that the results in Fig. 5 are consistent with the previous discussion of the mean Sherwood number. For example, the condition  $\gamma = 1480 \text{ s}^{-1}$  used in Fig. 5 gives  $A_f^2 \text{Pe}_\gamma = 1.5 \times 10^8$  for a resist thickness of  $h = 1 \text{ mm}$  and diffusivity  $D = 10^{-11} \text{ m}^2/\text{s}$ . A feature size of 200  $\mu\text{m}$  at this thickness yields  $A_f = 5$ , and Fig. 3 gives  $\text{Sh} \approx 3$  for these values. Thus the development time should lie about one-third of the way between the kinetic-limited and diffusion-limited times, as shown in Fig. 5.

Development times for acoustic agitation are shown in Fig. 6. These results are based on an acoustic intensity of  $I \sim 10 \text{ W}/\text{cm}^2$ . Again the bottom dose is always  $5.2 \text{ kJ}/\text{cm}^3$ .

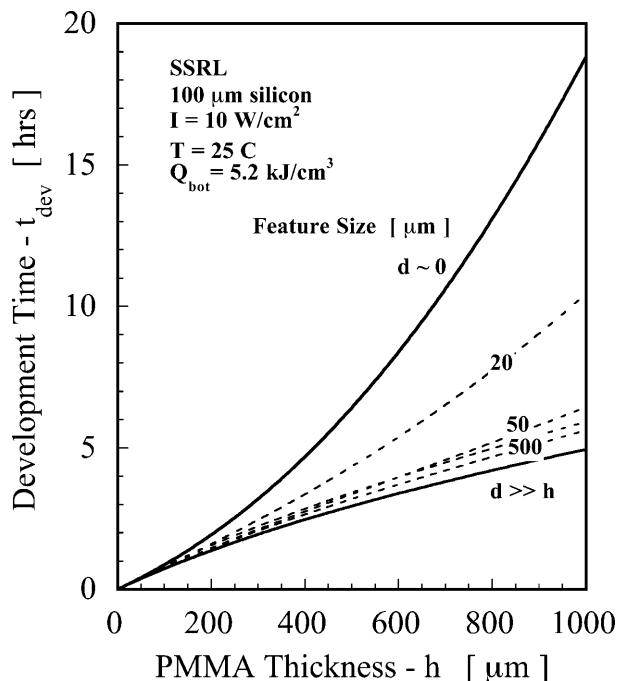


Fig. 6. Development times under acoustic agitation. Development times and time differentials are dramatically reduced for all aspect ratios when feature sizes are above about 20  $\mu\text{m}$

For acoustic agitation, we see that development times are reduced to nearly the kinetic-limited values for all feature sizes greater than about 50  $\mu\text{m}$ , and this is nearly independent of the resist thickness. Such behavior is consistent with the previous discussion of mean Sherwood numbers. At a resist thickness of  $h = 1 \text{ mm}$ , a feature size of 50  $\mu\text{m}$  corresponds to an aspect ratio of 20 and an acoustic intensity of  $10 \text{ W}/\text{cm}^2$  corresponds to  $A_f \text{Pe}_a = 440$ . For these conditions, the mean Sherwood number given in Fig. 4 is just over 10. Thus the development time should be near the kinetic-limited value. For a feature size of 20  $\mu\text{m}$ , however, the aspect ratio is  $A_f = 50$  at  $h = 1 \text{ mm}$ . In this case, the mean Sherwood number is only about 2.4 for the same intensity, so the development time should lie about halfway between the kinetic-limited and diffusion-limited times. This is also consistent with the results in Fig. 6.

## 7 Summary

For a first-order reaction governing dissolution kinetics, we find that the required overall development time for LIGA resists can be expressed as the sum of a kinetic-limited development time and a characteristic time for PMMA fragment transport. The kinetic-limited time depends only on the resist thickness, dose profile and development temperature. It is independent of feature size and aspect ratio when secondary radiation is neglected. The transport time varies with the square of the resist thickness and inversely with the PMMA fragment diffusivity and the mean Sherwood number. This transport time depends on the dose and development temperature only through their respective influences on the fragment diffusivity.

To compute these transport times, a new analytical model was developed to describe Sherwood numbers for features of high aspect ratio. We show that local Sherwood numbers for forced convective transport can be expressed in terms the instantaneous aspect ratio and a Peclet number based on the square of the feature size and the fluid shear rate just outside the feature. The Sherwood number does not vary with the aspect ratio, however, but depends instead only on the number of re-circulating cells spanning the feature depth. The number of cells is roughly the aspect ratio divided by 1.4 and rounded up to the nearest integer. Results of this model are in good agreement with measured Sherwood numbers for features located on a rotating disk.

We find that local Sherwood numbers do not increase smoothly with the Peclet number, except for aspect ratios less than about 1.4. Rather, they exhibit a series of relatively abrupt increases followed by plateaus. Each plateau spans about two orders of magnitude in the Peclet number. Local Sherwood numbers are also quite small when the aspect ratio is large. For aspect ratios above four, the Sherwood number does not exceed two for Peclet numbers up to  $10^5$ .

Feature aspect ratios vary continuously during the course of development, so local Sherwood numbers cannot accurately describe the effects of transport on overall development times. To avoid this, we define a mean Sherwood number based on the final aspect ratio; this mean value can be used directly in estimating the impact of transport on development times. Mean Sherwood numbers are presented as a function of the final aspect ratio for both forced convective transport and acoustic agitation. We find that the mean Sherwood number for forced convective transport is less than three for conditions of practical interest at all aspect ratios above five; it is less than two for aspect ratios above 10. Based on this, we conclude that forced convective transport will provide only very modest benefit in reducing development times or in improving uniformity of development times across features of differing size for aspect ratios above about five. For aspect ratios of 10 or more, the benefit is negligible. The benefit of forced convective transport will be even smaller for electrodeposition since high Peclet numbers are more difficult to obtain in this case. This is because the Schmidt number for metal ions in aqueous solution is about three orders of magnitude lower than that for PMMA fragments in developer. However, forced convective transport may still be of value in electrodeposition for LIGA mask fabrication since feature aspect ratios on masks are usually small.

In contrast, acoustic agitation under practical conditions can provide mean Sherwood numbers in excess of 10 for aspect ratios up to about 20. Such large values can dramatically reduce development times and should provide good uniformity over a range of feature sizes by

largely eliminating the transport limitation on development time.

## References

1. Becker EW; Ehrfeld W; Hagmann P; Maner A; Munchmeyer D (1986) Fabrication of microstructures with high aspect ratios and great structural heights by synchrotron radiation lithography, galvanofarming and plastic moulding (LIGA process). *Microelectro Eng* 4: 35–56
2. Munchmeyer D; Ehrfeld W (1987) Accuracy limits and potential applications of the LIGA technique in integrated optics. *Proc SPIE, Micromachining Ele Opt Submicrometer Dimen Surf Specific* 803: 72–79
3. Schmalz O; Hess M; Kosfeld R (1996) Structural changes in poly(methyl methacrylate) during deep-etch X-ray synchrotron radiation lithography. Parts I, II, III. *Die Angewandte Makromolekulare Chemie* 239: 63–106
4. Pantenburg FJ; Mohr J (1995) Influence of Secondary effects on the structure quality in deep X-ray lithographie. *Nucl Instrum Meth Phys Res B* 97: 551–556
5. Zanghellini J; El-Kholi A; Mohr J (1997) Development behavior of irradiated microstructures. *Microelectronic Eng* 35: 409–412
6. Zanghellini J; Achenbach S; El-Kholi A; Mohr J; Pantenburg FJ (1998) New development strategies for high aspect ratio microstructures. *Microsyst Technol* 4: 94–97
7. Pan CT; Yang H; Wang HJ; Chou MC (1999) Behavior of the developing process for ultradeep microstructures. *Sensors and Materials* 11: 339–347
8. Higdon JJJ (1985) Stokes flow in arbitrary two-dimensional shear flow over ridges and cavities. *J Fluid Mech* 159: 195–226
9. Shehata AK; Yang JD; West AC; Modi V (1999) Effect of unsteady external flow on transfer to cavities. *Int J Heat Mass Trans* 42: 673–683
10. Griffiths SK; Nilson RH; Bradshaw RW; Ting A; Bonivert WD; Hachman JT; Hruby JM (1998) Transport limitations in electrodeposition for LIGA microdevice fabrication. *Proc SPIE, Micromachining and Microfabrication Proc Technol IV* 3511: 364–375
11. Clift R; Grace JR; Weber ME (1978) *Bubbles Drops and Particles*. Academic Press, New York
12. Schlichting H (1968) *Boundary-Layer Theory*. McGraw-Hill, New York
13. Bade K; Leyendecker K; Thommes A; Bacher W (1995) Electroplating at high aspect ratio micro-patterned electrodes – influence of mass transfer. Fourth International Symposium of Magnetic Materials, Processes and Devices, Proceedings of the Electrochemical Society Fall Meeting, Chicago, USA
14. Nilson RH; Griffiths SK; Ting A (2001) Modeling acoustic agitation for enhanced development of LIGA PMMA resists. Fourth International Workshop on High-Aspect-Ratio Micro-Structure Technology (HARMST), Baden-Baden, Germany
15. Tan MX; Bankert MA; Griffiths SK; Ting A; Boehme DR; Wilson S; Balsler LM (1998) PMMA dose studies at various synchrotron sources and exposure/development conditions. *Proc SPIE, Materials and Device Characterization in Micromachining* 3512: 262–270
16. Pantenburg FJ; Achenbach S; Mohr J (1998) Influence of developer temperature and resist material on the structure quality in deep X-ray lithography. *J Vac Sci Technol B* 16: 3547–3551